AERODYNAMIC DESIGN OF A SUPERSONIC TRANSPORT CONFIGURATION CONSIDERING AVERAGE LOUDNESS IN THE WHOLE BOOM CARPET

Qing Chen[1,2], Zhong-Hua Han[1,2,*], Jian-Ling Qiao[1,2], Yu-Lin Ding[1,2], Ke-Shi Zhang [1,2] & Wen-Ping Song[1,2]

[1]Institute of Aerodynamic and Multidisciplinary Design Optimization, School of Aeronautics, Northwestern Polytechnical University, Xi'an, 710072, China
[2]National key Laboratory of Aircraft Configuration Design, Xi'an 710072, China

Abstract

Sonic booms remain the primary barrier restraining the development of supersonic transport (SST). The existing low-boom design methods primarily focus on mitigating under-track sonic boom intensity, which may increase the loudness at off-track locations in the sonic boom carpet. To solve this problem, a low-boom design method which can reduce the sonic boom across the whole boom carpet is proposed. First, the sonic boom prediction method is introduced and validated by the JWB configuration of SBPW2. Then, an average loudness metric termed full-carpet boom loudness (FBL) is formulated, which can consider the contribution of loudness and impact area at different off-track angles. By integrating the FBL and surrogate-based optimization, a full-carpet low-boom design optimization method is proposed. Finally, the proposed method is applied to the aerodynamic design of a low-boom SST configuration. After design, the sonic booms at all off-track angles are mitigated. The FBL is reduced from 80.79 PLdB to 79.84 PLdB and maximum loudness reduction in the carpet is 1.96 PLdB. The shock wave pattern of designed configuration is softer and the tail shocks are weakened. Additionally, the cruise lift-to-drag ratio is also improved by 2.3%. The design configuration maintains favorable low-boom characteristics at off-design conditions of ±0.1 Mach number and ±0.1° angle of attack off the design point. This research can provide insight for the low-boom design of SST configurations.

Keywords: supersonic transport, sonic boom, low-boom design, design optimization, sonic boom carpet

1. Introduction

Supersonic transport (SST) can double the cruise speed, which significantly improves travel efficiency. This makes it one of the most attractive directions for next-generation civil airliners[1]. However, sonic booms remain the primary environmental and operational barrier restraining the development of SSTs. SSTs drop a sonic boom carpet with a width of 60 to 80 kilometers on the ground during cruise, where all the creatures and buildings will suffer the huge loudness[2]. Therefore, reducing the sonic boom at any location in the whole boom carpet to an acceptable level is a critical problem that urgently needs to be addressed.

Currently, there are two main types of low-boom design method: inverse design and direct numerical optimization methods[3]. The inverse design methods reduce sonic boom by shaping the aircraft to match a given low-boom target distribution[4] (equivalent area or near-field overpressure distribution). Inverse design methods involve classic JSGD method, CFD-based near-field overpressure inverse design method, and mixed-fidelity method. Existing research proves that combining these three methods can achieve better low-boom design results[1]. Currently, inverse design methods are relatively mature[5] and have been successfully applied to the design of some advanced low-boom configurations[6]. Direct numerical optimization methods can be classified into 3 types based on their algorithms, including gradient-based, surrogate-based and evolution optimization. Among them, gradient-based optimization combined with adjoint method is very efficient[7], while surrogate-based optimization has good global optimization capability[8]. Both of them are widely used in low-boom

design optimization. For a long time, low-boom design methods mainly focus on the under-track sonic boom, as it was deemed to be strongest due to the shortest propagation distance[9].

However, researches have shown that refined under-track low-boom design can lead to stronger off-track sonic booms[10]. Consequently, there has been an increasing attention to low-boom designs for off-track booms in the carpet. In 2009, Plotkin[11] extended the classic JSGD theory using multipole analysis[12] method to generate low-boom targets at off-track angles. In 2015, Ordaz et al.[13] optimized the sonic boom characteristics at 25° off-track angle of C25 demonstrator using an adjoint method. Subsequently, Ueno et al.[14] used the second derivative and envelope of the inverse equivalent area distributions as design targets to reduce off-track booms[15]. Kirz[16] mitigated the maximum sonic boom intensity in the whole sonic boom carpet. However, these design methods only consider single off-track angle and have not consider the sonic boom characteristics across the whole carpet, often leading to increased sonic boom intensities at other locations.

In summary, existing low-boom design methods cannot account for the full-carpet boom characteristics, resulting in greater boom intensities at other off-track angles. Therefore, an average loudness metric termed FBL is proposed to evaluate the boom characteristics in the whole boom carpet. Based on this metric, a full-carpet low-boom design optimization method is proposed and applied to the aerodynamic design of a low-boom configuration. This research can provide insight for the low-boom design of SST configurations.

2. Methodology

2.1 Sonic boom prediction method

In this paper, computational fluid dynamics (CFD) simulation coupled with augmented Burgers equation is used for full-carpet sonic boom prediction. The procedure of sonic boom prediction is as follows. First, CFD simulation is employed to obtain the near-field sonic boom signatures at different off-track angles. Second, ray tracing method is used to determine the cutoff angle of the propagation. Third, near-field signatures within the cutoff angle are propagated to the ground using the augmented Burgers equation to predict the far-field sonic boom signatures. Finally, the ground loudness is calculated.

For near-field sonic boom prediction, Reynolds-Averaged Navier-Stokes (RANS) equations with SA turbulence model are solved for near-field boom simulation. The time discretization implemented using the LU-SGS implicit scheme. The inviscid fluxes are discretized using a second-order Roe upwind scheme. Besides, to precisely capture the shocks, a typical Mach-aligned strategy is used to generate CFD mesh for minimizing numerical dissipation.

For far-field prediction, the sonic boom is propagated along acoustic rays, which is determined by the following differential equation:

$$\begin{aligned} \frac{\mathrm{d}\mathbf{R}}{\mathrm{d}t} &= c_0\mathbf{n} + \mathbf{w} \\ \frac{\mathrm{d}\mathbf{n}}{\mathrm{d}t} &= -(\mathbf{I} - \mathbf{n}\otimes\mathbf{n}^{\mathrm{T}})\nabla(c_0 + \mathbf{w}\cdot\mathbf{n}) \end{aligned} \tag{1}$$

Then, the augmented Burgers equation is solved along these rays, accounting for nonlinear, dissipation and molecular relaxation effects, which is of the form：

$$\frac{\partial p'}{\partial s} = -\frac{1}{2G}\frac{\partial G}{\partial s}p' + \frac{\beta p'}{\rho_0 c_0^3}\frac{\partial p'}{\partial t'} + \frac{\delta}{2c_0^3}\frac{\partial^2 p'}{\partial t'^2} + \sum_j \frac{(\Delta c)_j \tau_j}{c_0^2\left(1+\tau_j\frac{\partial}{\partial t'}\right)}\frac{\partial^2 p'}{\partial t'^2} \tag{2}$$

After obtaining the ground sonic boom signatures, the perceived loudness level (PLdB) of the signature is calculated using the Stevens Mark VII method. In this paper, both the calculation of the far-field signatures and their loudness are calculated by using an in-house sonic boom prediction code named bBoom[17].

The full-carpet prediction method is validated by the JWB configuration from the 2nd AIAA Sonic Boom Prediction Workshop (SBPW2)[18]. The geometry of JWB is shown in Figure 1 (a). The mesh used for CFD simulation is shown in Figure 1 (b), and the number of cells is 28 million. The signatures at 3 body lengths (3BL) from the aircraft at different off-track angles are compared with the results of SBPW2 workshop. As shown in Figure 2, the calculated values are in good agreement with the reference values.

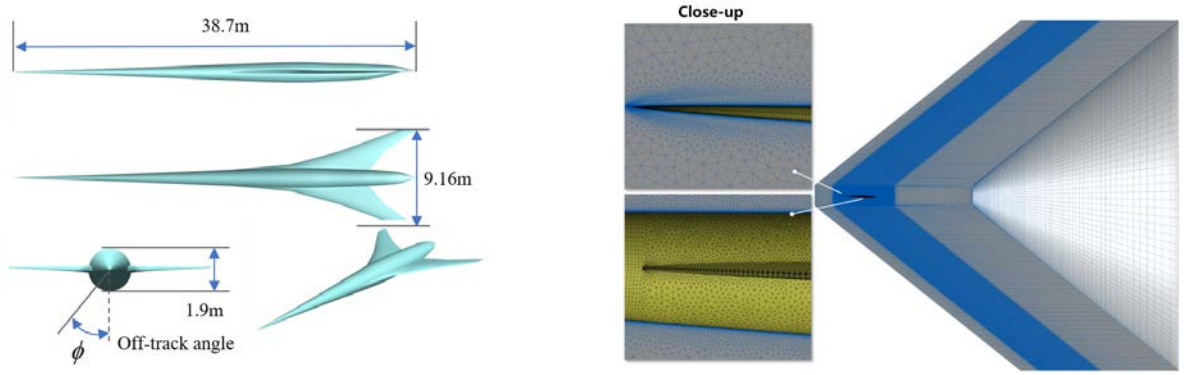

(a) Geometry of JWB (b) Mesh of JWB

Figure 1 – The geometry and mesh of JWB configuration

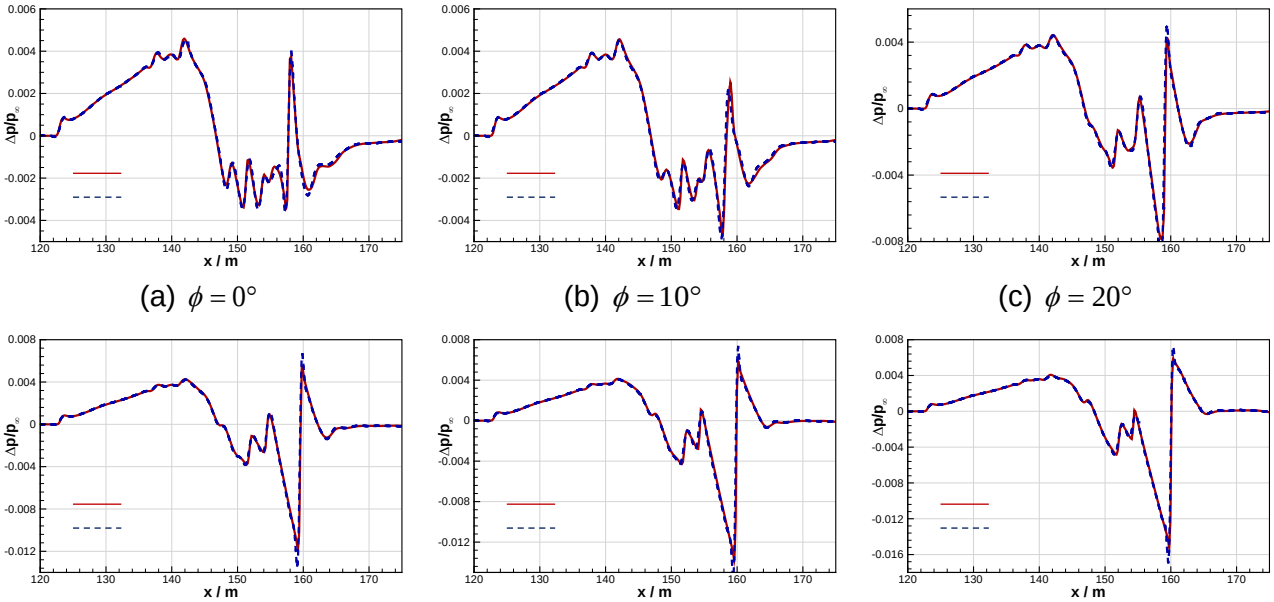

(a) $\phi = 0°$ (b) $\phi = 10°$ (c) $\phi = 20°$

(d) $\phi = 30°$ (e) $\phi = 40°$ (f) $\phi = 50°$

Figure 2 –Near-field signatures comparison between calculated and reference values[18]

These signatures are propagated to the ground and the loudness are calculated. The PLdB results compared with those published by the SBPW2 workshop are listed in Table 1. The maximum difference is 0.59 PLdB, and the minimum difference is only 0.06 PLdB. This validates the accuracy of the sonic boom prediction method used in the following design process.

Table 1 – Loudness comparison of calculated and reference values in the whole boom carpet

Azimuth angles	$\phi = 0°$	$\phi = 10°$	$\phi = 20°$	$\phi = 30°$	$\phi = 40°$	$\phi = 50°$
Calculated / PLdB	79.56	76.49	77.60	82.31	81.40	76.63
Reference / PLdB	79.50	76.74	78.08	82.01	81.37	76.24

2.2 Formulation of the optimization objective

The range of the sonic boom impact area within off-track angles of 0° to 5° is merely 1.56 km; while width drastically increases to 9.92 km for angles between 45° and 50°. Therefore, the bigger the off-track angle is, the wider the impact area. To consider both the width of the impact area and intensity of the sonic booms, a new metric named full-carpet sonic boom loudness (FBL) is formulated, which is defined by the expression:

$$\mathrm{FBL} = \frac{1}{2y_0}\int_{-y_0}^{y_0} f_{dB}(y)dy \tag{3}$$

In Equation (5), $f_{dB}(y)$ is metric for the sonic boom intensity, such as PLdB, ASEL, or CSEL sound

level; y_0 denotes the lateral coordinate of the cut-off point, which means the width of the carpet is $2y_0$.The FBL not only accounts for the distribution of acoustic energy at each off-track angle but also considers the impact area at these angles across the sonic boom carpet, thereby serving as an metric for the full-carpet sonic boom intensity. Moreover, by dividing the integral by the width of the boom carpet, the dimensionality of FBL is ensured to be consistent with that of the boom intensity measured at a single off-track angle. In practice, the number of off-track angles to extract near-field signatures is finite, so the integral can be numerically solved using the trapezoidal rule.

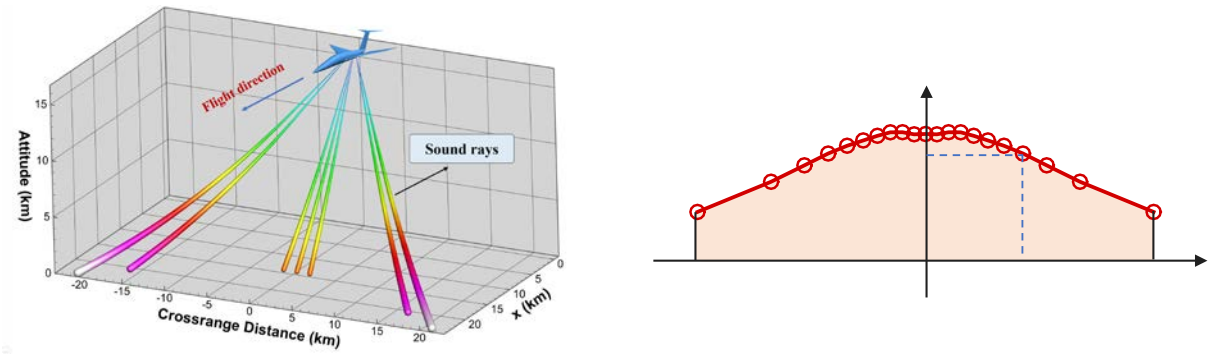

(a) The propagating sound rays (b) Formulation of FBL

Figure 3 – Metric of full-carpet sonic boom characteristics

2.3 Full-carpet low-boom design optimization method

The flowchart of proposed full-carpet low-boom design optimization method in this paper is shown in the Figure 4. The process is as follows:

Step1: Input and parametrize the baseline configuration.

Step2: CFD simulations are conducted to calculate near-field sonic boom signatures within the cutoff off-track angles.

Step3: The near-field signatures are propagated to the ground to get PLdB distribution across the boom carpet, and the FBL is calculated.

Step4: An inhouse optimizer named SurroOpt[19] is used to minimize the FBL.

Step5: Output the optimum design configuration.

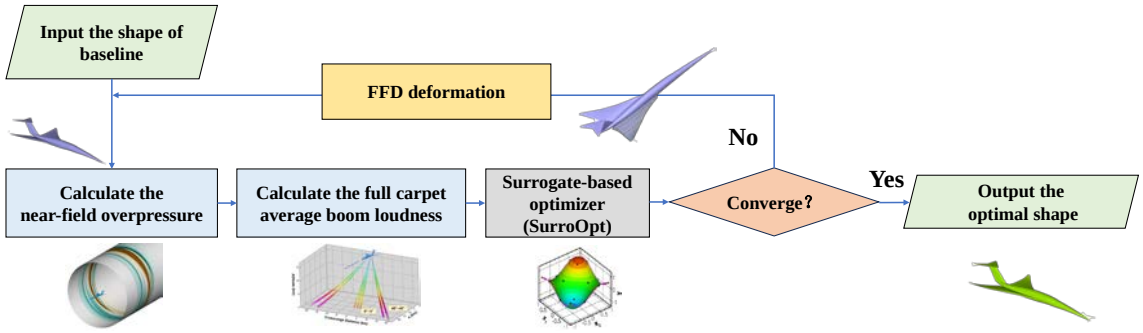

Figure 4 – The flowchart of the full-carpet low-boom design optimization method

3. Full-carpet low-boom design of an SST configuration

3.1 Baseline configuration and optimization model

The baseline is a 20-PAX SST configuration[20] under the flight condition of M = 1.6, whose under-track loudness is 79.88 PLdB, and maximum PLdB is at 15° off-track angle. Figure 5 presents the parameters, geometry and boom characteristics of the baseline. The wing is parametrized with FFD (Free-form deformation) method and 6 control profiles along the spanwise are chosen as design variables to describe the dihedral distribution of the wing. Since both the upper and lower surface control points are shifted at the same time, the thickness of the wing can remain constant during the optimization.

Parameter	Value
Fuselage length	45 m
Wing area	130 m²
Take-off weight	30 t
Cruise Mach number	1.6
Cruise C_L	0.112
Cruise altitude	16,000 m

(a) Parameters

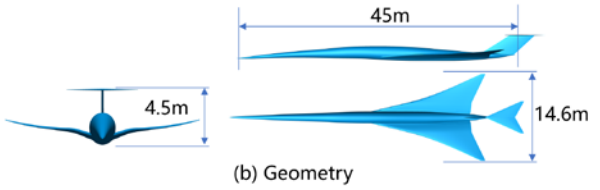

(b) Geometry

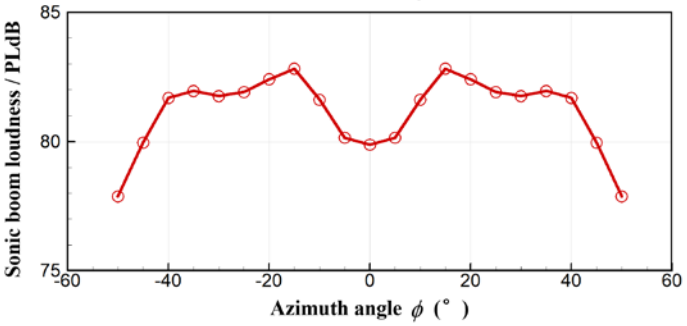

(c) Sonic Boom characteristics

Figure 5 – The baseline configuration

The optimization model is as follows:

$$\begin{aligned} \min \quad & f = \mathrm{FBL} \\ s.t. \quad & h_{i,L} \le h \le h_{i,U} \ (i = 1,2,\cdots,6) \\ & C_L \ge C_{L,0} \\ & PLdB_{\phi=0^\circ}^{design} \le PLdB_{\phi=0^\circ}^{baseline} + 1 \end{aligned} \tag{4}$$

Where, $h_{i,L}$, $h_{i,u}$ are the lower and upper bounds of FFD control points respectively; $C_{L,0}$ is the cruise lift coefficient. Additionally, a constraint of under-track loudness is imposed, which can maintain the under-track boom characteristic which has been specially designed. In the optimization process, the latin hypercube sampling is selected for the design of experiments (DoE), and expected improvement (EI) infill-sampling criterion is used to repetitively select new samples to update the kriging model. The initial number of samples is 20, and the maximum number of samples is 100.

3.2 Results of design optimization

Geometry comparison of the baseline and design configurations is shown in Figure 6 (a). After the optimization, the wing dihedral of the inner segment is reduced, whereas the relative dihedral of the outer wing segment is increased. This can distribute the energy of shocks to all off-track angles.

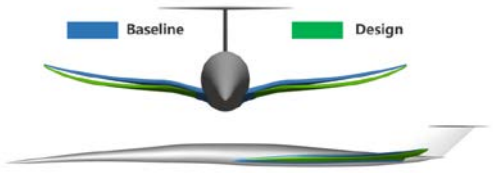

(a) Geometry comparison

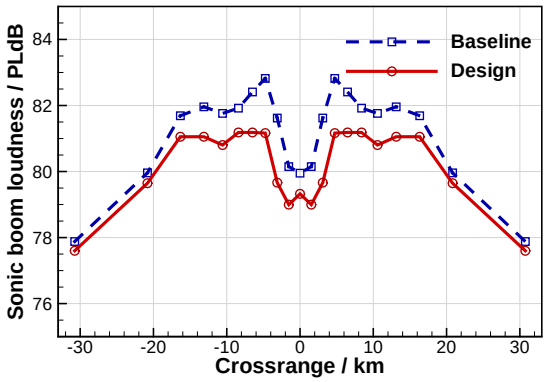

(b) Sonic boom loudness comparison

Figure 6 – Geometry and sonic boom loudness comparison of the baseline configuration

Figure 6 (b) shows a comparison of PLdB distribution in the whole boom carpet. It is evident that the loudness of the design configuration is lower than that of the baseline across the whole boom carpet. Specifically, the maximum sonic boom on the carpet is decreased from 82.82 PLdB to 81.16 PLdB, while the maximum boom reduction is at 3.10 km laterally (10° off-track angle) with a loudness reduction 1.96 PLdB.

3.3 Analysis of the design configuration

3.3.1 Sonic boom characteristics

Figure 15 presents the density gradient of axial direction on the cylindrical surface at a distance of 135m away from the aircraft, demonstrating that the shock pattern along the off-track direction of design configuration is softer. Specifically, an expansion wave is introduced at x = 210 m to tailor the strong shock wave into two weaker shocks along the off-track direction. Furthermore, behind the axial distance of 217 m, additional shock/expansion wave structures are introduced into the flow field, leading to favorable interference which can mitigates the intensity of the aft-body wave system.

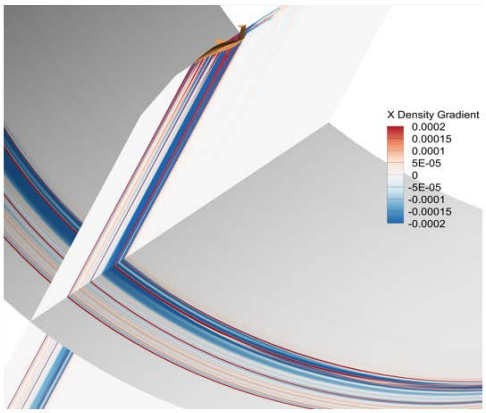

(a) Cylinder surface (R=135m)

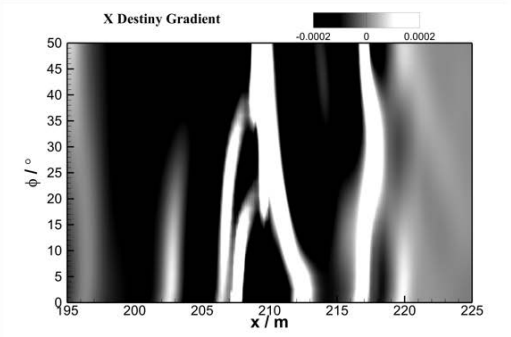

(b) X density gradient (baseline)

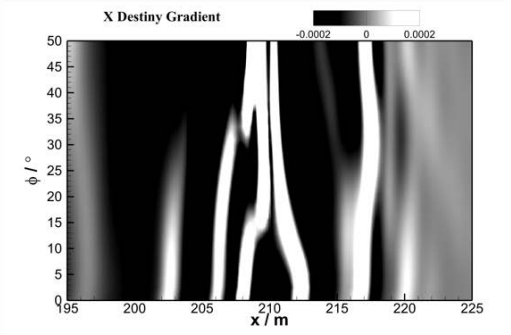

(c) X density gradient (design)

Figure 7 – Shock wave patterns of the baseline and design configuration

Due to the fact that the reduction of the loudness within off-track angles ranging from 0° to 15° is most significant, so the near- and far-field sonic boom signatures at these directions are compared and analyzed, as shown in Figure 8 and Figure 9. To maintain the cruise lift, an enhanced compression due to lower surface of the wing leads to a stronger shock wave at x = 188 m. This effect is more evident in the far-field that the peak of overpressure is higher of the design configuration. However, due to the softer aft-body shocks of the design configuration, there is a notably increased rise time of the tail shock in the far-field signatures. This can fetch a significant decrease in medium and high frequency components of acoustic energy, which contributes to a reduction in the PLdB of ground signatures. This is the mechanism that the ground loudness of design configuration is lower than that of baseline at all locations in the boom carpet.

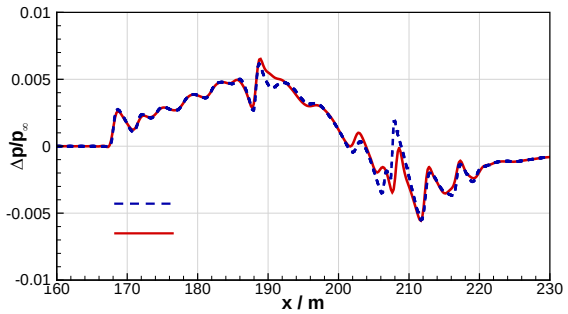

(a) $\phi = 0°$

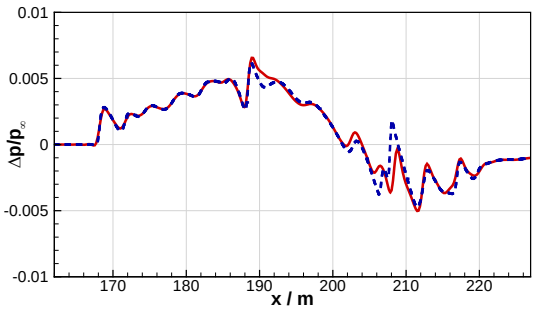

(b) $\phi = 10°$

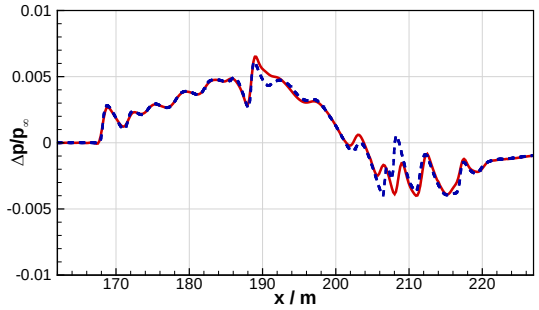

(c) $\phi = 20°$

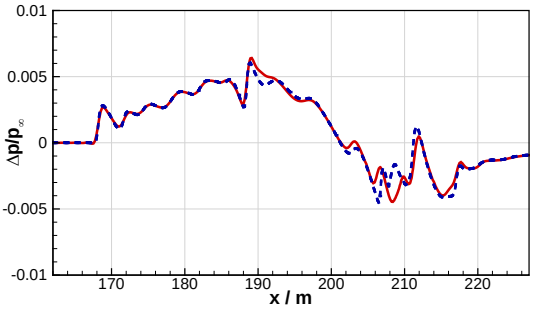

(d) $\phi = 30°$

Figure 8 – Near-field signatures comparison of the baseline and design configuration

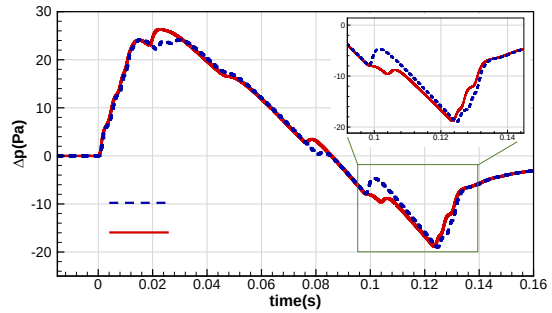

(a) $\phi = 0°$

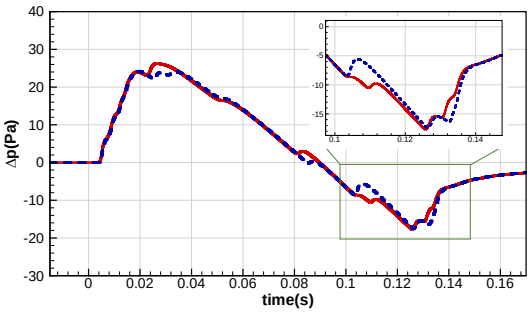

(b) $\phi = 10°$

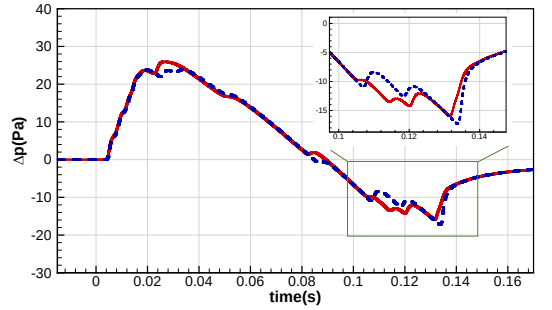

(c) $\phi = 20°$

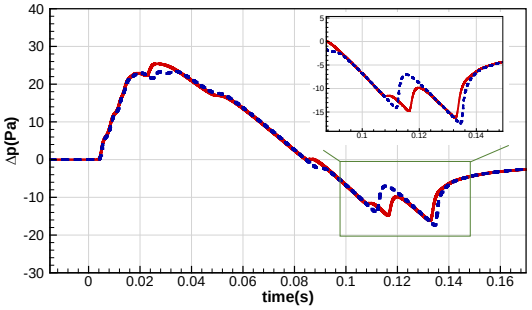

(d) $\phi = 30°$

Figure 9 – Far-field signatures comparison of the baseline and design configuration

3.3.2 Aerodynamic characteristics

The aerodynamic performance of design configuration is analyzed. As shown in Figure 10, the surface pressure coefficient Cp contours of design configuration is similar to the baseline. This means alteration in aerodynamic performance is slight after the full-carpet low-boom optimization.

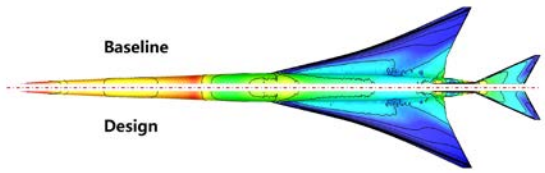

(a) Upper surface

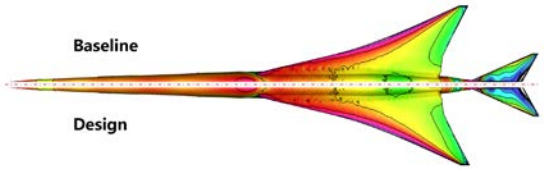

(b) Lower surface

Figure 10 – Surface pressure distribution comparison between baseline and design configuration

Figure 11 presents a comparison of the aerodynamic characteristics before and after the design optimization. Owing to the enhanced compression on the lower surface of the wing, the design configuration outperforms the baseline in lift characteristics. Specifically, the cruise lift coefficient has increased from 0.112 to 0.114, while the drag coefficient has decreased by 0.5 counts. This leads to an improvement in both lift characteristic and aerodynamic efficiency.

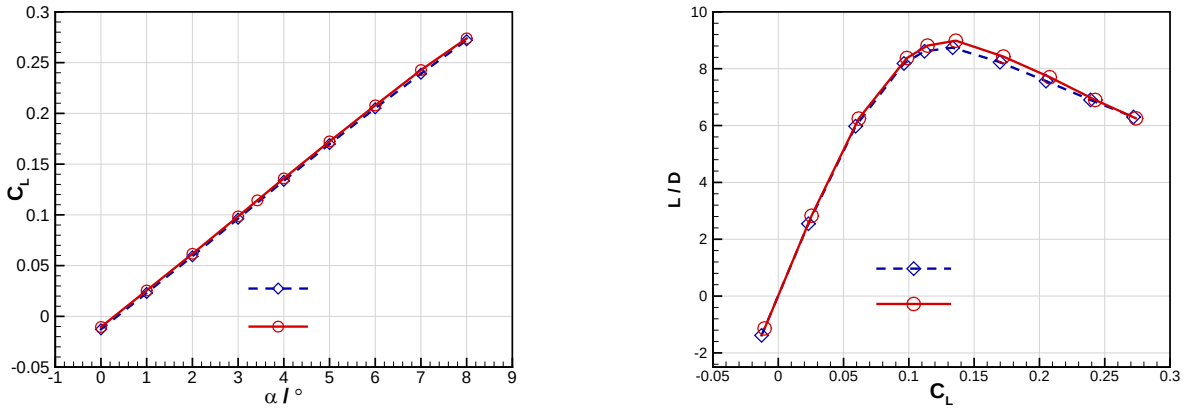

(a) lift characteristic (b) lift-to-drag ratio characteristic

Figure 11 – Aerodynamic characteristics comparison of the baseline and design configuration

3.4 Off-design sonic boom characteristics

To evaluate the off-design sonic boom characteristics of the design configuration, the ground loudness at different Mach numbers and angles of attack are calculated. The Mach numbers and angles of attack are varied by ±0.1 (in steps of 0.05) and ±0.1° (in steps of 0.05°) respectively. It should be noted that, perturbations in angle of attack and Mach number lead to changes in aircraft attitude and Mach angle, which means the CFD mesh must be re-generated in order to accurately simulate the sonic boom. Additionally, since acoustic rays propagate perpendicular to Mach cone, variations in Mach numbers also influence the width of the sonic boom carpet. Lateral cutoff angles and widths of the boom carpets at different Mach numbers are calculated and listed in Table 2.

Table 2 – Width of sonic boom carpet at different Mach number

Ma	ϕ_{cutoff} / °	Crossrange / km
1.50	48.0°	60.89
1.55	49.0°	59.79
1.60	50.0°	61.50
1.65	51.2°	69.16
1.70	51.9°	69.34

The results are shown in Figure 12. It is worth to be noted that the ground loudness is very sensitive to speed increments for every off-track angle. Take the under-track sonic boom as an example, when the Mach number is 1.65, the maximum PLdB under varying angles of attack reaches 82.44 PLdB. When the Mach number is 1.7, this maximum PLdB increases dramatically to 85.15 PLdB.

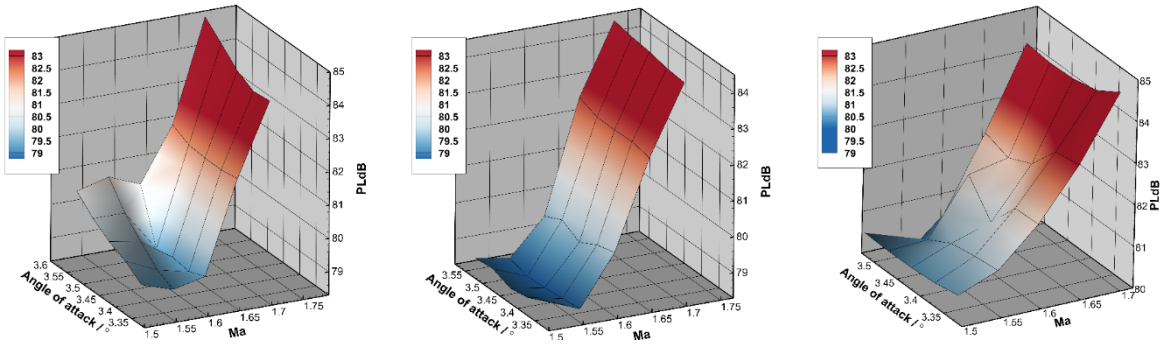

(a) $\phi = 0°$ (b) $\phi = 10°$ (c) $\phi = 20°$

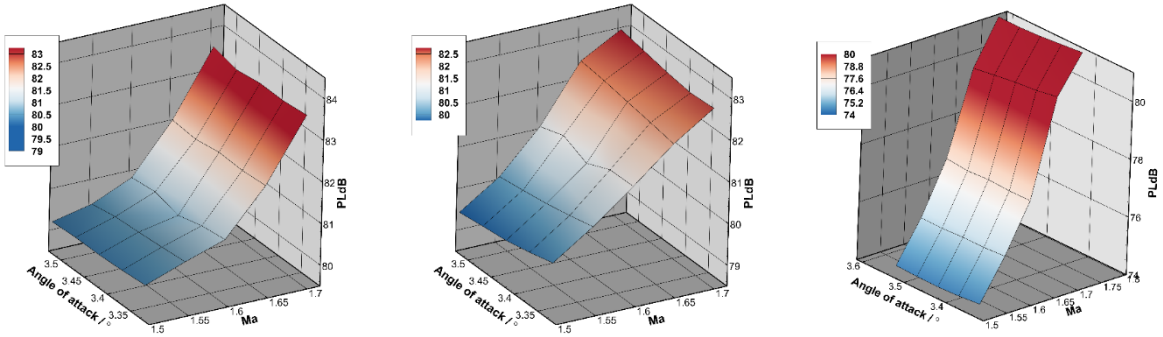

(d) $\phi = 30°$ (e) $\phi = 40°$ (f) $\phi = 50°$

Figure 12 – PLdB distributions at different off-track angles

Figure 13 presents PLdB distributions in the sonic boom carpet as a function of angle of attack at different Mach numbers. It can be concluded that the intensity of the under-track boom is more sensitive to angle of attack. This phenomenon is due to the fact that the propagation distance for under-track boom is shortest, so nonlinear and dissipation effects are less evident than those off-track directions. Consequently, perturbations in the near-field signatures due to angle of attack have a more evident impact on the far-field sonic boom intensity.

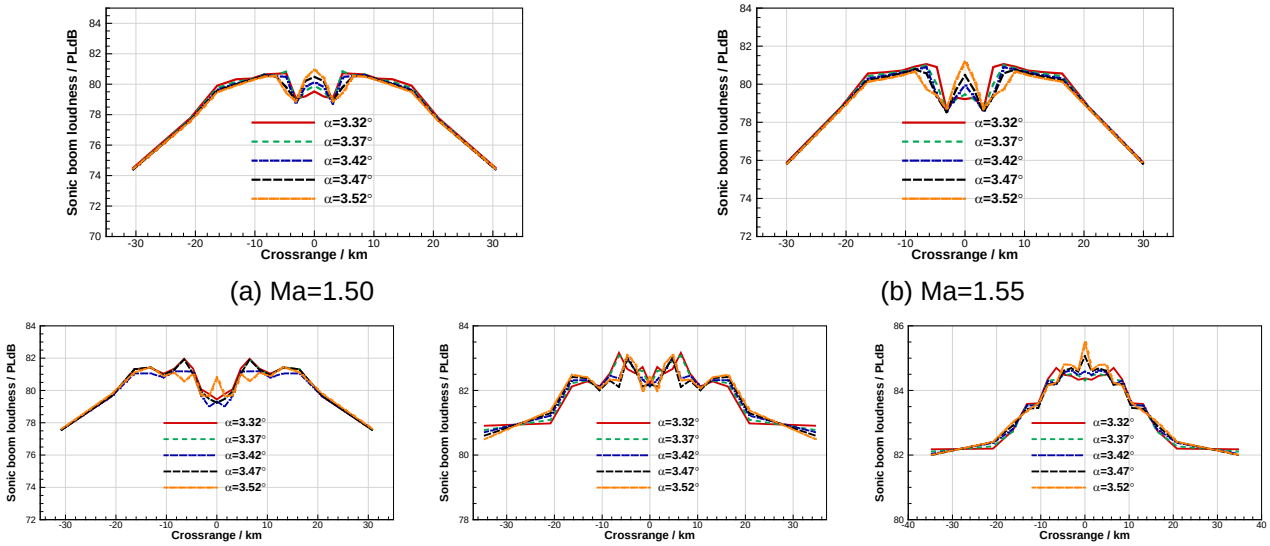

(a) Ma=1.50 (b) Ma=1.55

(c) Ma=1.60 (d) Ma=1.65 (e) Ma=1.70

Figure 13 – PLdB distributions in the sonic boom carpet at different Mach number

When the flight conditions deviate from the design point within the range of ±0.05 Mach numbers and ±0.1° in angle of attack, the ground loudness is below 83PLdB, which means the design configuration maintains good low-boom characteristics.

4. Conclusion

To mitigate the sonic boom intensity in the whole boom carpet, a full-carpet low-boom design optimization method is proposed and applied to the design of a low-boom SST configuration. To evaluate the sonic boom characteristics in the whole boom carpet, an average loudness metric termed FBL is formulated. By integrating the ground loudness across the carpet, the boom intensity and impact area at various off-track angles can be considered simultaneously. Combing the FBL with surrogate-based optimization, a full-carpet low-boom design optimization method is proposed. This method is applied to the aerodynamic design of a 20 PAX SST low-boom configuration, and the sonic boom intensity of design configuration is mitigated at all locations in the whole boom carpet. By optimizing the wing dihedral distribution, the tail shocks of far-field signatures are weakened, with a maximum ground loudness reduction of 1.96 PLdB. Additionally, the design configuration has a good aerodynamic and off-design sonic boom performance.

For future research, the sonic boom minimization theory considering full-carpet characteristics needs further investigation. Moreover, the full aircraft geometry will be parametrized and designed, and the aeroelastic deformation as well as engine intake-exhaust effects will be considered at the same time.

5. Acknowledge

This work was supported by the National Natural Science Foundation of China (No.12072285 & 5247120887), the Youth Innovation Team of Shaanxi Universities, and the National Key Research and Development Program of China under Grant No. 2023YFB3002800. The work was carried out at National Supercomputer Center in Xi'an, and the calculations were performed on Sugon.

6. Contact Author Email Address

Zhong-Hua Han, Professor, hanzh@nwpu.edu.cn, corresponding author.

7. Copyright Statement

References

[1] Han Z H, Qiao J L, Zhang L W, et al. Recent progress of efficient low-boom design and optimization methods. *Progress in Aerospace Sciences*, Vol. 146, No. 101007, 2024.

[2] Maglieri D J, Bobbitt P J, Plotkin K J, et al. Sonic boom: Six decades of research: NASA SP-622 [R]. Hampton: NASA, 2014.

[3] Li W, Geiselhart K. Multidisciplinary design optimization of low-boom supersonic aircraft with mission constraints. *AIAA Journal*, Vol. 59, No. 1, pp 165-179, 2021.

[4] Ordaz I, Li W. Using CFD surface solutions to shape sonic boom signatures propagated from off-body pressure. *31st AIAA Applied Aerodynamics Conference*, San Diego, CA, No. 2660, pp 1-10, 2013.

[5] Li W, Rallabhandi S K. Inverse design of low-boom supersonic concepts using reversed equivalent-area targets. *Journal of Aircraft*, Vol. 51, No. 1, pp 29-36, 2014.

[6] Ding Y L, Han Z H, Qiao J L, et al. Inverse design method for low-boom supersonic transport with lift constraint. AIAA Journal, Vol. 61, No. 7, pp 2840-2853, 2023.

[7] Nemec M, Aftosmis M. Parallel adjoint framework for aerodynamic shape optimization of component-based geometry. *49th AIAA Aerospace Sciences Meeting*, Orlando, Florida, No. 1249, pp 1-26, 2011.

[8] Jim T M, Faza G A, Palar P S, et al. A multiobjective surrogate-assisted optimisation and exploration of low-boom supersonic transport planforms. *Aerospace Science and Technology*, Vol. 128, No. 107747, 2022.

[9] Zhang L W, Han Z H, Qiao J L, et al. Effect of longitudinal lift distribution on sonic boom of a canard-wing-stabilator-body configuration. *Chinese Journal of Aeronautics*, Vol. 36, No. 9, pp 92-108, 2023.

[10] Ordaz I, Li W. Integration of off-track sonic boom analysis for supersonic aircraft conceptual design. *Journal of Aircraft*, vol. 51, No. 1, pp 23-28, 2014.

[11] Plotkin K J. Sonic boom shaping in three dimensions. *30th AIAA Aeroacoustics Conference*, Miami, Florida, No. 3387, pp 1-13, 2009.

[12] George A R. Reduction of sonic boom by azimuthal redistribution of overpressure. *AIAA Journal*, Vol. 7, No.2, pp 291-298, 1969.

[13] Ordaz I, Wintzer M, Rallabhandi S K. Full-carpet design of a low-boom demonstrator concept. *33rd AIAA Applied Aerodynamics Conference*, Dallas, TX, No. 2261, pp 1-15, 2015.

[14] Ueno A, Kanamori M, Makino Y. Robust low-boom design based on near-field pressure signature in whole boom carpet. *Journal of Aircraft*, Vol. 54, No. 3, pp 918-925, 2017.

[15] Ueno A, Makino Y. Robust low-boom design in primary boom carpet. *AIAA Scitech 2021 Forum,* Virtual Event, No. 1270, pp 1-15, 2021.

[16] Kirz J. Surrogate-based low-boom low-drag nose design for the JAXA S4 supersonic airliner. *AIAA SCITECH 2022 Forum*, San Diego, CA, No. 0706, pp 1-12, 2022.

[17] Qiao J L, Han Z H, Ding Y L, et al. Far-field sonic boom prediction considering atmospheric turbulence effects: An improved approach. *Chinese Journal of Aeronautics*, Vol. 35, No. 9, 208-225, 2022.

[18] Park M A, Nemec M. Nearfield summary and statistical analysis of the second AIAA sonic boom prediction workshop. *Journal of Aircraft*, Vol. 56, No. 3, pp 851-875, 2019.

[19] Han Z H. SurroOpt: A generic surrogate-based optimization code for aerodynamic and multidisciplinary design. *30th ICAS*, Daejeon, Korea, pp 1-10, 2016.

[20] Chen Q., Han Z H, Ding Y L, et al. Low-boom design of T-tail supersonic transport configuration. *14th Asia Pacific International Symposium on Aerospace Technology*, Ling shui, Hai nan,. pp 1-10, 2023.